Global Warming Pattern Formation: The Role of Ocean Heat Uptake

SHINENG HU,[a] SHANG-PING XIE,[b] AND SARAH M. KANG[c]

[a] *Division of Earth and Climate Sciences, Nicholas School of the Environment, Duke University, Durham, North Carolina*
[b] *Scripps Institution of Oceanography, University of California San Diego, La Jolla, California*
[c] *School of Urban and Environmental Engineering, Ulsan National Institute of Science and Technology, Ulsan, South Korea*

(Manuscript received 20 April 2021, in final form 22 November 2021)

ABSTRACT: This study investigates the formation mechanism of the ocean surface warming pattern in response to a doubling CO_2 with a focus on the role of ocean heat uptake (or ocean surface heat flux change, ΔQ_{net}). We demonstrate that the *transient* patterns of surface warming and rainfall change simulated by the dynamic ocean–atmosphere coupled model (DOM) can be reproduced by the *equilibrium* solutions of the slab ocean–atmosphere coupled model (SOM) simulations when forced with the DOM ΔQ_{net} distribution. The SOM is then used as a diagnostic inverse modeling tool to decompose the CO_2-induced thermodynamic warming effect and the ΔQ_{net} (ocean heat uptake)–induced cooling effect. As ΔQ_{net} is largely positive (i.e., downward into the ocean) in the subpolar oceans and weakly negative at the equator, its cooling effect is strongly polar amplified and opposes the CO_2 warming, reducing the net warming response especially over Antarctica. For the same reason, the ΔQ_{net}-induced cooling effect contributes significantly to the equatorially enhanced warming in all three ocean basins, while the CO_2 warming effect plays a role in the equatorial warming of the eastern Pacific. The spatially varying component of ΔQ_{net}, although globally averaged to zero, can effectively rectify and lead to decreased global mean surface temperature of a comparable magnitude as the global mean ΔQ_{net} effect under transient climate change. Our study highlights the importance of air–sea interaction in the surface warming pattern formation and the key role of ocean heat uptake pattern.

KEYWORDS: Air-sea interaction; Climate change; Hydrologic cycle; Surface fluxes; Surface temperature; Climate models

1. Introduction

Greenhouse warming features considerable spatial variations in both observations and model simulations. For example, surface warming is polar amplified over land surface and sea ice, but it tends to be suppressed over the Southern Ocean (Manabe et al. 1990; Marshall et al. 2015; Armour et al. 2016; Singh et al. 2018; Hill et al. 2020) and the subpolar North Atlantic (Drijfhout et al. 2012; Gervais et al. 2019; Hu and Fedorov 2020). In the tropics, abundant regional warming patterns modulate regional rainfall change (Xie et al. 2010). Understanding how the warming pattern forms is critical for determining Earth's climate sensitivity and for the projection of regional climate change (Armour et al. 2013; Xie 2020; Garuba et al. 2018; Dong et al. 2020). For the historical period, a portion of the observed global warming pattern comes from the spatially varying radiative forcing induced by short-lived aerosols that are typically regionally confined (Mitchell et al. 1995; Shindell and Faluvegi 2009). However, it is important to note that CO_2 alone can also induce a global warming pattern (Manabe et al. 1990), with similarities and differences to that arising from aerosols (Wang et al. 2016; Deser et al. 2020).

Using ensembles of CO_2-doubling simulations with an atmospheric general circulation model, Dong et al. (2009) estimate that sea surface temperature (SST)-forced response explains 80% and 64% of the land surface temperature in December and June, respectively, with the rest being explained by the direct CO_2 forcing with an unchanged SST. SST is therefore a vital factor that determines land surface temperature changes and shapes global warming pattern. Many factors, however, can influence SST, including both atmospheric and oceanic processes (Fig. 1). Atmospheric changes in, for example, surface winds and clouds can perturb the ocean surface energy budget and modify SST. At the same time, changes in ocean heat transport convergence into the ocean mixed layer due to, for example, ocean circulation or mixing can also modify SST. Oceanic and atmospheric processes are not independent, and they actively communicate with each other via heat, freshwater, and momentum fluxes at the air–sea interface.

Understanding the coupling of oceanic and atmospheric processes is therefore critical to deciphering the global warming SST pattern formation. A key quantity to the ocean–atmosphere coupling is the net ocean surface heat flux, hereafter denoted as Q_{net}, consisting of longwave and shortwave radiative fluxes and latent and sensible turbulent heat fluxes. Hu et al. (2020) investigate the formation mechanism of the global pattern of Q_{net} change (ΔQ_{net}, or ocean heat uptake) in response to a doubling CO_2 and find that ocean circulation changes play an important role in shaping the ΔQ_{net} pattern, partially compensated for by the passive advection effect induced by the mean circulation.

In the current study, we aim to take a step further to explore the connection between ΔQ_{net} and the surface warming pattern. The effects of ocean heat uptake on surface temperature and tropical rainfall changes have been extensively

Corresponding author: Shineng Hu, shineng.hu@duke.edu

DOI: 10.1175/JCLI-D-21-0317.1

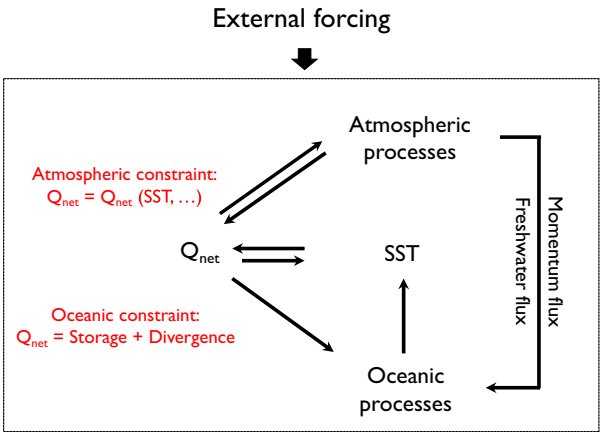

FIG. 1. A schematic of ocean–atmosphere coupled system response to external forcing. The Q_{net} serves as a key quantity that couples the ocean and the atmosphere, and is fundamentally constrained by oceanic and atmospheric processes. Adopted from Hu et al. (2020).

studied with slab ocean–atmosphere coupled models (SOMs), often in idealized settings for conceptual understanding (e.g., Broccoli et al. 2006; Yoshimori and Broccoli 2008; Kang et al. 2008, 2009; Hwang and Frierson 2013; Bischoff and Schneider 2014; Kang and Xie 2014; Rose et al. 2014; Rose and Rayborn 2016; Haugstad et al. 2017; Hwang et al. 2017). Here we extend these studies by using the SOM as a diagnostic tool: take the ΔQ_{net} pattern from the dynamic ocean–atmosphere coupled model (DOM) transient response to CO_2 increase and explore its effect on surface warming and rainfall change patterns. A similar modeling approach has also been used to study the impact of ocean heat uptake on time-evolving radiative feedbacks (Rugenstein et al. 2016) and polar amplification (Singh et al. 2017). The SOM-based diagnostic modeling framework complements the approach of Tomas et al. (2016) to understand how ocean heat transport change alters the SST response to Arctic sea ice loss.

The paper is organized as follows. Section 2 describes the model and the experimental design. In particular, we use a SOM as a diagnostic inverse modeling tool to infer global warming pattern, with the results presented in section 3. The impact of ocean heat uptake on the warming pattern and tropical rainfall change is further decomposed in section 4. We summarize our key findings and discuss the implications in section 5.

2. Model and experimental setup

a. Model

We use the Community Earth System Model (CESM) version 1.2.2.1 developed by the National Center for Atmospheric Research (NCAR). The atmospheric component, the Community Atmosphere Model version 4 (CAM4; Neale et al. 2010), uses a spectral grid at a spatial resolution of about 3.7° both latitudinally and longitudinally. The ocean component, the Parallel Ocean Program version 2 (POP2; Smith et al. 2010), uses a displaced-pole grid at a spatial resolution of 3.6° longitudinally and approximately 1.6° latitudinally that is refined in the tropics and varies in space. The model has active land, sea ice, and ice sheet components. More details about the model can be found in Gent et al. (2011). Here we choose a low-resolution configuration and an older version of the atmospheric component due to the limitation of computational resources. The robustness of our results will need to be tested with a higher-resolution configuration, updated model physics (e.g., Rugenstein et al. 2016; Singh et al. 2017; Liu et al. 2018a,b; Lin et al. 2021), and other climate models.

Besides the regular DOM configuration, we also use the motionless SOM configuration where only a mixed-layer ocean is present (Bitz et al. 2012). In the SOM, a spatially and monthly varying heat flux, often called the Q-flux, is specified to account for the ocean heat transport effect due to the oceanic processes like advection and mixing. An annually averaged but spatially varying ocean mixed layer is used, which may cause some biases in the seasonal variations of SST over the high latitudes. Mixed layer temperature, or equivalently SST, is interactively calculated based on net surface heat flux variations. Both the Q-flux and mixed-layer depth are determined from DOM simulations. Sea ice model remains prognostic in all SOM simulations.

b. Experimental setup

We first perform two sets of DOM experiments, one for preindustrial control (DOM_CTL) and the other for global warming with an abrupt doubling of CO_2 (DOM_Cx2). Both sets of simulations use the initial conditions taken from the end of a long preindustrial control run over 500 years. Following the methodology in the CESM Large-Ensemble Project (Kay et al. 2015), we conduct 10 runs in each set of experiments starting from slightly different atmospheric initial conditions on the order of 10^{-14} K. Each experiment is integrated for 50 years. We choose the last 10 years of integration as an example transient stage following CO_2 doubling for further analysis. We realize that 100 years (i.e., 10 members, 10 years each) may still contain the signals of multidecadal internal climate variability, and future work with an increased ensemble size is needed to better isolate forced signals. Those DOM simulations will be used to inform the design of the SOM experiments as we will describe next.

We then conduct a series of SOM experiments that are forced by different combinations of CO_2 level and Q-flux. All the SOM experiments described below are integrated for 60 years each. Since it typically takes less than 10 years for a SOM simulation to equilibrate, we use the last 50 years to calculate the equilibrium climate.

We perform one preindustrial control simulation (SOM_CTL) and one CO_2-doubling simulation (SOM_Cx2), aiming to reproduce the corresponding DOM climate states. We compute the ensemble-mean Q_{net} climatology from the last 10 years of the DOM experiments and prescribe it as the spatially and monthly varying Q-flux in their corresponding SOM

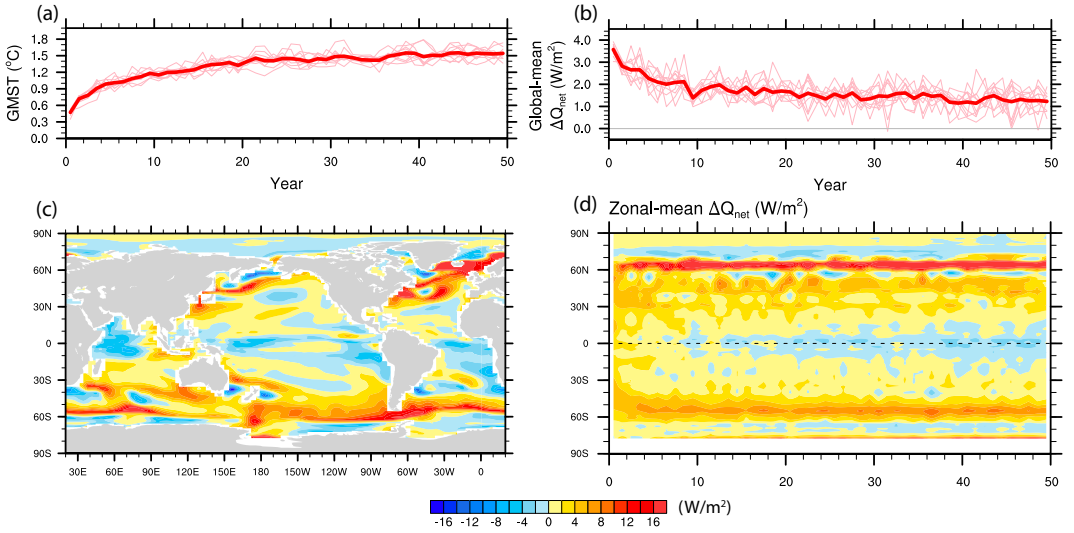

FIG. 2. Annual-mean global mean (a) surface temperature (GMST) and (b) net ocean surface heat flux change (ΔQ_{net}) for the DOM abrupt CO_2 doubling experiments. Thick red is for ensemble mean, and thin pink is for ensemble members. (c) Global map of annual-mean ΔQ_{net} averaged over years 41–50. (d) Hovmöller diagram of zonal-mean annual-mean ΔQ_{net} (W m^{-2}). In (c) and (d), ensemble-mean results are shown. The results are derived from DOM_Cx2 − DOM_CTL.

experiments. It is noteworthy that the global mean of Q_{net} is not removed, which as we will show later is critical to reproducing the climate in the DOM experiment. The annual-mean spatially varying, prescribed mixed-layer depth is also diagnosed from the corresponding DOM experiments.

To isolate the role of regional Q_{net} change under global warming, we construct various Q-flux forcing fields and apply them to the SOM simulations with the CO_2 doubling. In SOM_Cx2REF we use the Q_{net} diagnosed from DOM_CTL, representing the direct impact of CO_2 doubling in the absence of Q_{net} changes. The difference between SOM_Cx2 and SOM_Cx2REF stands for the impact of global Q_{net} changes. In SOM_Cx2NO, we combine the DOM_Cx2 Q_{net} for the northern oceans poleward of 30°N and the DOM_CTL Q_{net} for the rest of global oceans; a 5° linear buffering zone is added over 30°–35°N for a smooth transition. Subtracting SOM_Cx2REF from SOM_Cx2NO, we can isolate the climate impact of regional Q_{net} changes over the northern oceans. Similarly, we conducted SOM_Cx2SO and SOM_Cx2TO to isolate the impacts of the southern (poleward of 30°S) and tropical oceans (30°S–30°N) Q_{net} changes, respectively. Besides the regional decomposition as mentioned above, an alternative approach is to separate the global mean and spatially varying components of the Q_{net} changes. Comparing those two cases SOM_Cx2GM and SOM_Cx2SP, respectively, with the reference case SOM_Cx2REF, we can isolate the impacts of the global mean ΔQ_{net} and patterned ΔQ_{net}.

In all the SOM sensitivity experiments described above, the mixed-layer depth from DOM_CTL is used. Since the SOM simulations are integrated until equilibrium, the choice of mixed-layer depth should not largely affect the climate mean state.

3. Diagnostic modeling of global warming pattern

Climate response to the abrupt doubling of CO_2 unfolds in two stages, first a fast response that mainly accounts for the warming of the upper ocean and then a slow response involving the deep ocean changes (Fig. 2a; Held et al. 2010). Similarly, global mean ΔQ_{net} (downward positive) drops rapidly by about a half in the first few years from about 3.5 W m^{-2}—the radiative forcing associated with CO_2 doubling—and then gradually declines; it decreases to about 1.2 W m^{-2} by year 50 (Fig. 2b). The spatial structure of ΔQ_{net}, however, emerges quickly in less than a decade (Rugenstein et al. 2016; Garuba et al. 2018; Lin et al. 2021) and remains strong toward the end of the 50-yr simulation even as the global mean ΔQ_{net} decreases by a factor of 3 (Figs. 2c,d). The global pattern of ΔQ_{net} is dominated by positive values over high latitudes, mostly in the Southern Ocean and the North Atlantic, accompanied by weak negative values over the tropical oceans; in other words, ocean heat uptake mainly occurs over high-latitude oceans, while tropical oceans lose heat to the atmosphere.

On one hand, Q_{net} change is directly constrained by oceanic processes; see Hu et al. (2020) for a comprehensive diagnosis and discussion. Background ocean circulation and circulation changes both play important roles in shaping the global ΔQ_{net} pattern by generating anomalies in ocean heat transport, but their relative contributions vary in space and remain to be further reconciled (e.g., Banks and Gregory 2006; Xie and Vallis 2012; Winton et al. 2013; Marshall et al. 2015; Huber and Zanna 2017; Hu et al. 2020). On the other hand, the ΔQ_{net} pattern is also affected by atmospheric processes (surface wind speed, cloud cover, etc.), providing an atmospheric constraint. The ΔQ_{net} pattern is also suggested to be closely

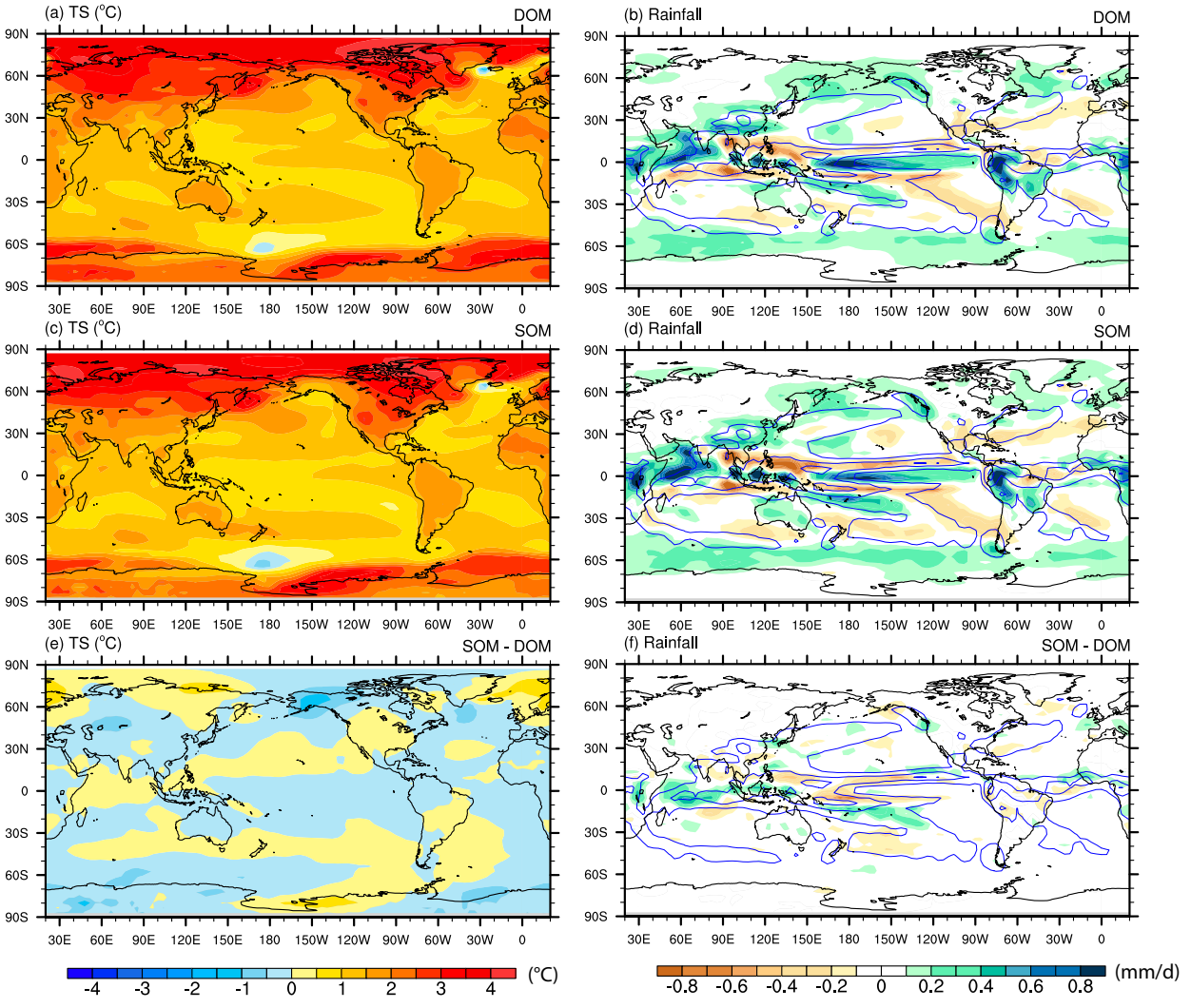

FIG. 3. (a),(b) Changes in annual-mean (a) surface temperature (°C) and (b) precipitation (mm day^{-1}) in response to the abrupt doubling of CO_2 in DOM (i.e., DOM_Cx2 − DOM_CTL). (c),(d) As in (a) and (b), but for SOM (i.e., SOM_Cx2 − SOM_CTL). In the rainfall panels, blue contours are for annual-mean climatological rainfall in SOM_CTL with an interval of 3 mm day^{-1}. (e),(f) The differences between SOM and DOM.

connected to the SST change pattern under global warming (e.g., Xie et al. 2010). A warmer SST favors stronger heat release to the atmosphere and thus tends to be associated with a more negative (i.e., upward) ΔQ_{net}.

Can we therefore reconstruct the transient SST pattern under global warming based on ΔQ_{net} information? SOM forced by the climatological Q-flux diagnosed from the Q_{net} field in DOM, has often been used to reproduce the equilibrium climate state simulated by DOM (e.g., Bitz et al. 2012). But it is not obvious whether and to what extent the *transient* climate change pattern in DOM can be reproduced by the *equilibrium* solutions in SOM, which will be explicitly tested next.

Figure 3a shows the transient warming pattern in DOM averaged over years 41–50 and across 10 ensemble members. For comparison, Fig. 3c shows the equilibrium warming pattern in SOM averaged over years 11–60. In general, SOM simulations forced by the DOM ΔQ_{net} can reproduce quite well the global warming amplitude and pattern simulated by the DOM. The global mean surface temperature (GMST) increase is 1.53°C for the DOM and 1.48°C for the SOM, with an error of 3%. The key warming features of the DOM simulations that are captured in the SOM simulations include, for example, the polar amplification, the suppressed warming over the Southern Ocean and the subpolar North Atlantic, and the enhanced warming over the equatorial oceans. Although the ΔQ_{net} forcing is applied over oceans only, land surface warming pattern can also be well reproduced, suggesting a strong remote control by SSTs. The global pattern correlation in surface temperature change between DOM and SOM is 0.96. The mismatches are found mainly over high latitudes (Fig. 3e), perhaps related to the fact that the DOM

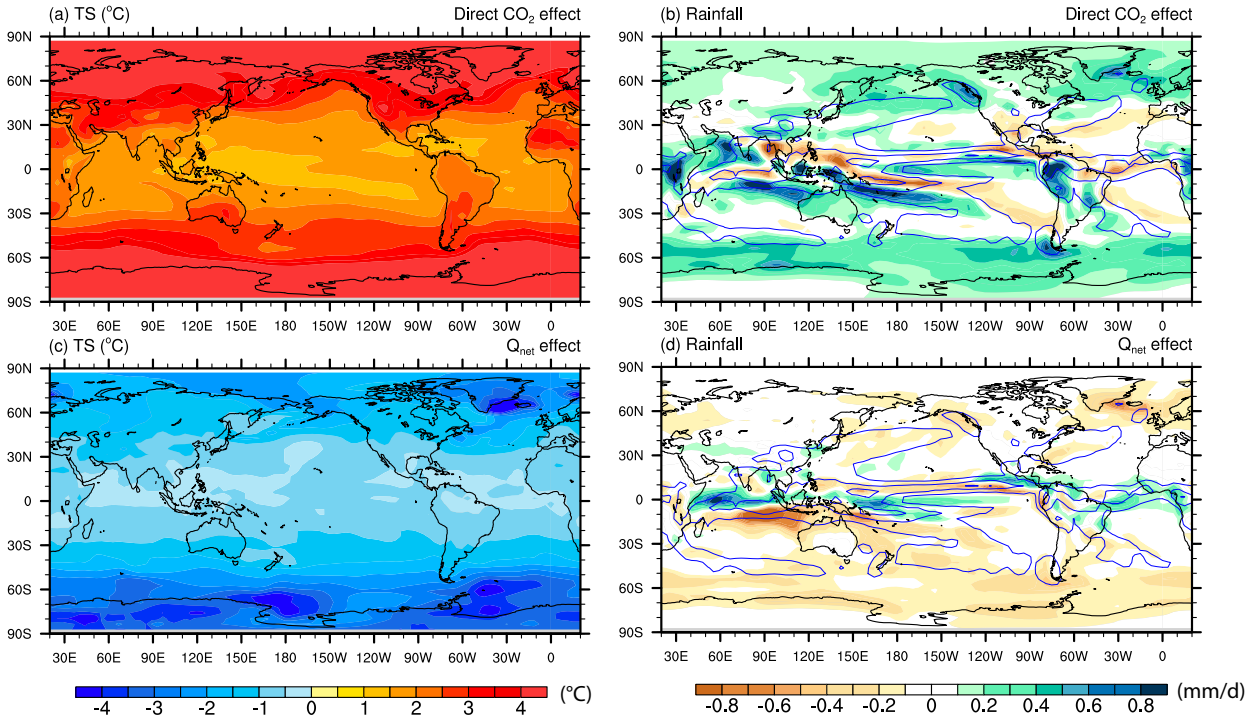

FIG. 4. Changes in annual-mean (left) surface temperature (°C) and (right) precipitation (mm day^{-1}) associated with (a),(b) the direct CO_2 effect in the absence of Q_{net} changes and (c),(d) the ΔQ_{net} effect. The direct CO_2 effect is derived from SOM_Cx2REF − SOM_CTL. The ΔQ_{net} effect is derived from SOM_Cx2 − SOM_Cx2REF. In the rainfall panels, blue contours are for annual-mean climatological rainfall in SOM_CTL with an interval of 3 mm day^{-1}.

interannual sea ice variability, not fully represented in the SOM, can potentially affect the mean climate through nonlinear processes (e.g., sea ice–albedo feedback).

The DOM-simulated rainfall change pattern can also be reasonably reproduced by the SOM, including the enhanced rainfall over the equatorial Pacific, the northward shift of South Pacific convergence zone (SPCZ), the northward shift of intertropical convergence zone (ITCZ) over the Indian Ocean, the reduced rainfall in the subtropics, and the enhanced rainfall over the high latitudes (Figs. 3b,d). The largest mismatches in rainfall change are located in the tropical Indo-western Pacific (Fig. 3f), where local SST has a strong control on rainfall variability and SST gradient may play a role as well (Fig. 3e; also see Back and Bretherton 2009; He et al. 2017; Duffy et al. 2020).

Singh et al. (2017) also used CESM1 but with an updated, higher-resolution atmospheric component, CAM5, and investigated the climate state 300 years after CO_2 abrupt doubling, presumably closer to equilibrium than our case. Nevertheless, they found that CO_2 doubling produced a significantly stronger warming in their SOM than in DOM by about 12% in terms of GMST. It is not clear what has caused the larger SOM–DOM discrepancy in their simulations. Further tests with other climate models are needed. It is important to emphasize here that, in order for the SOM to reproduce the transient climate change simulated by the DOM, a key step is to keep the global mean ΔQ_{net} in the Q-flux forcing. Otherwise, the SOM will produce a warm bias, because the cooling effect due to the globally nonzero heat uptake by the deep ocean is artificially removed. This point will be further illustrated in section 4c.

4. Attributing the global warming pattern: Surface temperature and rainfall

Using the SOM, we have successfully transformed an initial-value problem (i.e., transient climate response to CO_2 forcing) to a boundary-value problem (i.e., equilibrium climate state given CO_2 forcing and Q-flux). This transformation of framework makes it easier to further attribute the climate change pattern to the contributions of different factors at any transient stage of global warming.

a. Isolating the effects of CO_2 forcing versus ΔQ_{net}

We first isolate the effect of CO_2 forcing in the absence of Q_{net} changes and the effect of ΔQ_{net} on global surface temperature and rainfall pattern; hereafter we will call them the direct CO_2 effect and ΔQ_{net} effect, respectively. The direct CO_2 effect here involves SST changes, associated with a fixed Q_{net}, and it should therefore be distinguished from "the direct CO_2 effect in the absence of SST changes" sometimes used in the literature. Without the ΔQ_{net} effect, the doubling of CO_2 alone induces a much warmer climate with a GMST increase of 2.70°C (Fig. 4a). In this case, polar amplification becomes even more prominent in both hemispheres and the

suppressed warming over the Southern Ocean and the subpolar North Atlantic disappears. The equatorially enhanced warming is weaker and only evident in the eastern equatorial Pacific.

We then consider the impact of ΔQ_{net}, here calculated as the difference between the net warming and the direct CO_2 effect. It is noteworthy that other studies (e.g., Singh et al. 2017) may directly impose the perturbed Q_{net} forcing to SOM without a CO_2 doubling to obtain the impact of global Q_{net} changes. How the effects of global Q_{net} changes depend on the background climate state, which is out of scope of this study, needs further investigations.

The value of Q_{net} varies substantially in space (Fig. 2c) and is primarily balanced by the ocean heat transport divergence in the local mixed-layer ocean (Xie et al. 2010). The global mean ΔQ_{net} during years 41–50 is about $+1.3$ W m^{-2}, suggesting that the heat uptake by the deep ocean acts to cool the mixed layer ocean. As a result, the ΔQ_{net} effect acts to damp the global warming and cools the GMST by 1.22°C (Fig. 4c). The ΔQ_{net}-induced cooling is found everywhere in the globe, including over the tropical oceans where ΔQ_{net} is mostly negative (i.e., oceanic processes acting to warm the mixed-layer ocean) and over land where no direct ΔQ_{net} is imposed. The land–sea contrast in surface temperature changes due to the ΔQ_{net} effect is much weaker than that due to the direct CO_2 effect.

Interestingly, the CO_2 warming effect and the ΔQ_{net} cooling effect share strong spatial similarities with a global temperature pattern correlation of -0.82 (Figs. 4a,c). The similarities between the two are particularly evident when the surface temperature change is zonally averaged, both being largely polar amplified in the two hemispheres (Fig. 5a). Nevertheless, their underlying causes are different. For the CO_2 warming effect, since the CO_2 radiative forcing is largely uniform in space (Huang et al. 2017), the hemispherically symmetric, polar amplified surface warming is mostly determined by the meridional structure of net climate feedback, with maximum (negative) values in the tropics (e.g., Alexeev et al. 2005; Taylor et al. 2013; Armour et al. 2013; Park et al. 2018; Stuecker et al. 2018; Goosse et al. 2018). But unlike the direct CO_2 effect, ΔQ_{net} has substantial spatial variations and there exist two regional peaks with the same sign, one in the Southern Ocean and the other in the subpolar North Atlantic (Fig. 2c). In addition to the meridionally varying climate feedback, this particular spatial structure of ΔQ_{net} forcing allows it to produce an even more prominent pattern of polar amplification (Alexeev et al. 2005; Rose et al. 2014; Kang and Xie 2014). For example, the pole-to-equator ratio of surface temperature change is about 3.5 for the CO_2 warming effect but can reach 7 for the ΔQ_{net} cooling effect (Fig. 5a). The zonally integrated ΔQ_{net} over the Southern Ocean can be twice as large as that over the extratropical oceans in the Northern Hemisphere, due to its large spatial coverage [not shown; see Fig. 4 in our companion study, Hu et al. (2020)]. The ΔQ_{net} cooling effect is therefore particularly strong in the southern high latitudes, leading to the strongly muted Antarctic amplification as compared to Arctic amplification in the net warming (see the black lines in Fig. 5a).

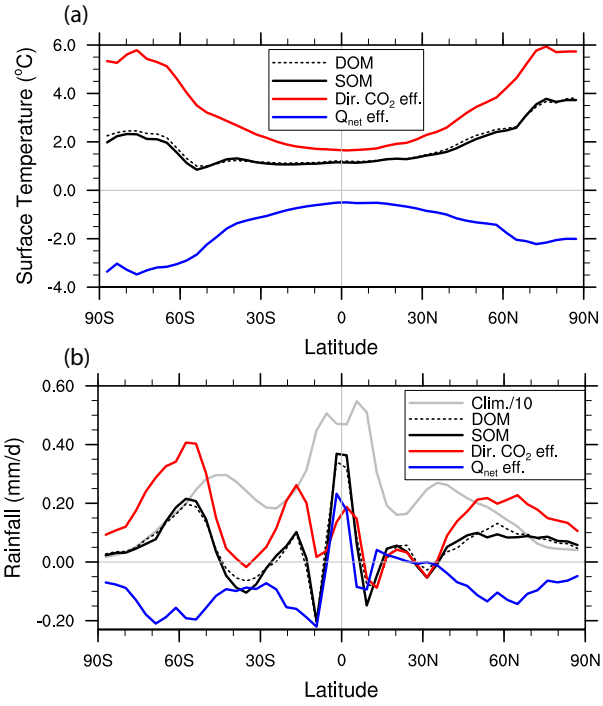

FIG. 5. Zonal-mean changes in annual-mean (a) surface temperature (°C) and (b) precipitation (mm day^{-1}) in different simulations. Here DOM is DOM_Cx2 − DOM_CTL, SOM is SOM_Cx2 − SOM_CTL, the CO_2 effect is SOM_Cx2REF − SOM_CTL, and the Q_{net} effect is SOM_Cx2 − SOM_Cx2REF. In (b), the gray line is for the climatological annual-mean precipitation divided by 10.

In terms of rainfall changes, the CO_2-induced warming effect results in a rainfall increase in most of the globe while the ΔQ_{net}-induced cooling effect produces a rainfall decrease in general (Figs. 4b,d). Their combined effect on the zonal-mean rainfall is characterized by an enhancement of equatorial rainfall with a reduction on either side and a poleward shift of midlatitudes rainfall belt (Fig. 5b), consistent with other climate models (Lau et al. 2013). Meridional variations in the extratropical rainfall response are nearly opposite for the direct CO_2 effect and the ΔQ_{net} effect, both peaking around 60°N and 60°S. In the tropics, however, they exhibit in-phase meridional variations with an equatorial peak. As we will demonstrate in section 4d, tropical rainfall changes experience strong zonal variations, and in fact, the similar equatorial enhancement of rainfall for the direct CO_2 effect and the ΔQ_{net} effect results from different causes.

b. Decomposing the effect of regional ΔQ_{net}

Next, we aim to understand how the regional ΔQ_{net} influences the global warming pattern. Two approaches have been proposed in the existing literature. In the first approach, regional Q-flux perturbations are applied in a SOM and the impacts of ocean heat uptake on global climate can directly be diagnosed. This approach has significantly advanced our

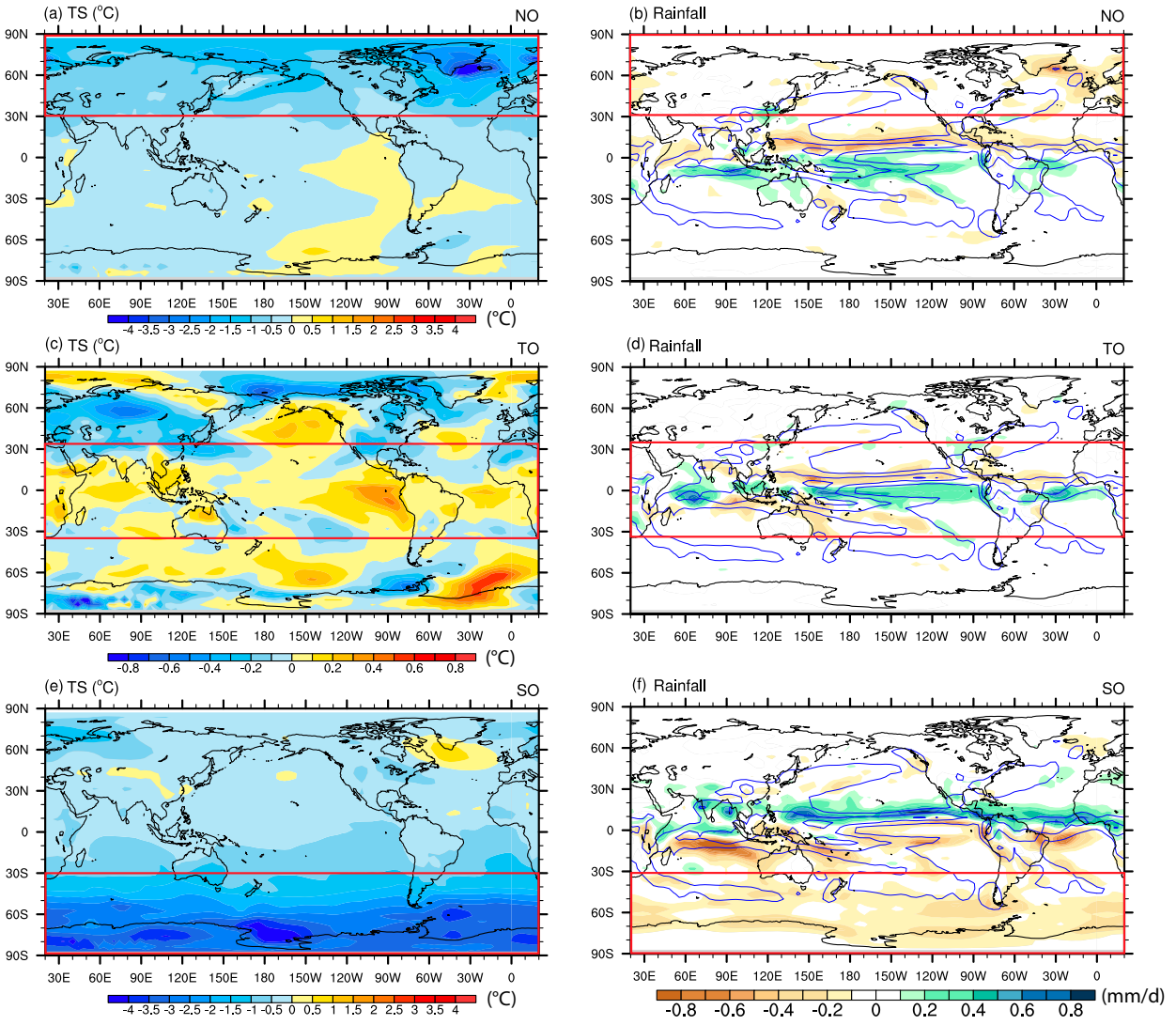

FIG. 6. Changes in annual-mean (left) surface temperature (°C) and (right) precipitation (mm day^{-1}) associated with the ΔQ_{net} effect of the (a),(b) northern oceans (SOM_Cx2NO − SOM_Cx2REF), (c),(d) tropical oceans (SOM_Cx2TO − SOM_Cx2REF), and (e),(f) southern oceans (SOM_Cx2SO − SOM_Cx2REF). In the rainfall panels, blue contours are for annual-mean climatological rainfall in SOM_CTL with an interval of 3 mm day^{-1}. Red boxes highlight the regions where ΔQ_{net} forcing is imposed. Note the different color bar in (c).

understanding of the impact of regional ocean heat uptake on, for example, hydrological cycle, climate sensitivity, and radiative feedbacks (Broccoli et al. 2006; Yoshimori and Broccoli 2008; Kang et al. 2008, 2009; Hwang and Frierson 2013; Bischoff and Schneider 2014; Kang and Xie 2014; Rose et al. 2014; Rose and Rayborn 2016; Haugstad et al. 2017; Hwang et al. 2017). In the second approach, a suite of SOM simulations with Q-flux patches are first conducted, and a linear Green's function is then used to reconstruct the climate impacts of regional ocean heat uptake in the area of interest (Liu et al. 2018a,b; Lin et al. 2021). Here we adopt the first approach with a particular focus on the impact of regional ocean heat uptake on global warming and rainfall change patterns.

We first divide the global ΔQ_{net} forcing into three regional ΔQ_{net} terms in different latitudinal bands and investigate their individual effects on global climate (Fig. 6). The Southern Ocean ΔQ_{net} exerts a particularly strong cooling impact in the Southern Hemisphere and the cooling extends toward the tropics (Figs. 6e and 7a), pushing the ITCZ northward evident over all three ocean basins (Figs. 6f and 7b) (Kang et al. 2008, 2009; Hwang and Frierson 2013; Hwang et al. 2017). The northern oceans ΔQ_{net} induces a relatively weaker cooling effect and it is mostly confined in the subpolar North Atlantic where the strongest forcing is located (Fig. 6a). The high-latitude cooling induced by the northern oceans ΔQ_{net} also reaches the tropics, leading to a southward shift of ITCZ that opposes the effect of Southern Ocean ΔQ_{net} (Figs. 6b and 7b).

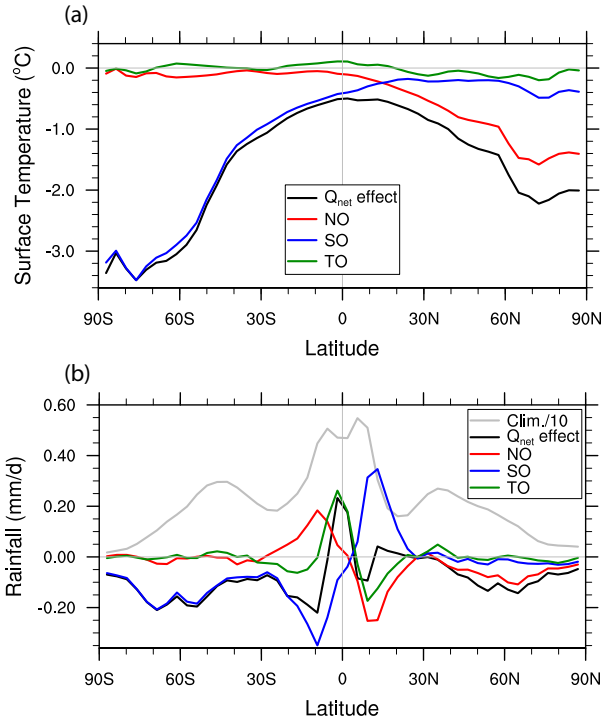

FIG. 7. Zonal-mean changes in annual-mean (a) surface temperature (°C) and (b) precipitation (mm day^{-1}) in different simulations. Here the Q_{net} effect is SOM_Cx2 − SOM_Cx2REF, NO is SOM_Cx2NO − SOM_Cx2REF, SO is SOM_Cx2SO − SOM_Cx2REF, and TO is SOM_Cx2TO − SOM_Cx2REF. In (b), the gray line is for the climatological annual-mean precipitation divided by 10.

The Southern Ocean ΔQ_{net}-induced cooling penetrates further into the deep tropics than the cooling induced by the northern oceans ΔQ_{net}, due to the blocking effect of a northward-displaced climatological ITCZ (Kang et al. 2020). The particular strong, far-reaching impacts of the Southern Ocean heat uptake is broadly consistent with the finding of Lin et al. (2021) from a linear Green's function and a series of "patch" SOM simulations (Liu et al. 2018a,b), with important implications for the temporal evolution of radiative feedbacks.

Another difference in the tropical response to northern versus southern extratropical forcing is that, the former gives rise to an El Niño–like pattern with a weakened zonal SST gradient, while the latter leads to a La Niña–like equatorial temperature change pattern with an enhanced zonal SST gradient (Figs. 6a,e). The difference in the response of tropical Pacific zonal SST gradient can potentially lead to distinctive radiative feedbacks through the modulation of cloud feedbacks as is suggested by previous studies (e.g., Zhou et al. 2017; Dong et al. 2019; Lin et al. 2021). Such differences in the tropical SST response are also suggested to be related to the northward displacement of the climatological ITCZ (Kang et al. 2020); note that although the model used here has a double ITCZ bias, the northern ITCZ is still more prominent than the southern one (Fig. 3b).

The tropical rainfall response to the tropical ocean ΔQ_{net} consists of a mixture of an equatorial enhancement and a southward ITCZ shift, the latter reinforcing the northern ocean ΔQ_{net} effect (Figs. 6d and 7b). The tropical rainfall changes in turn drive global surface temperature changes via atmospheric teleconnections (Fig. 6c). However, in terms of GMST, the impact of tropical ocean ΔQ_{net} is only within −0.01°C as a result of the strong cancellation of positive and negative values, while the impacts of northern and southern ocean ΔQ_{net} are significantly larger, −0.34°C and −0.81°C, respectively. The dominant control of the high-latitude ΔQ_{net}, as compared to the low-latitude ΔQ_{net}, on global climate is consistent with previous studies using various modeling approaches (e.g., Winton et al. 2010; Rose et al. 2014; Kang and Xie 2014; Rugenstein et al. 2016; Kang et al. 2017; Liu et al. 2018a,b; Stuecker et al. 2020; Lin et al. 2021). Although each ΔQ_{net} forcing in the three latitudinal bands separately induces a significant ITCZ migration, they largely cancel out and only leave an equatorial rainfall enhancement without a clear shift in the zonal-mean sense (Fig. 7b).

It is important to note that here we use the SOM as a diagnostic tool to isolate the impact of regional ΔQ_{net}, which itself results partly from dynamical air–sea coupling. If a DOM is used instead, the ITCZ shift response to high-latitude forcing may become much muted, due to the dynamical air–sea coupling in the tropics (Kay et al. 2016; Green and Marshall 2017; Schneider 2017; Kang et al. 2018; Wang et al. 2018). These DOM experiments provide meaningful physical insights with applications to understanding, for example, the tropical rainfall response to Arctic or Antarctic sea ice loss (England et al. 2020).

c. *The role of global mean ΔQ_{net} versus patterned ΔQ_{net}*

Different methods of ΔQ_{net} decomposition can provide complementary views on the role of ΔQ_{net} in shaping the global warming pattern. An alternative, meaningful way to decompose ΔQ_{net} is to separate its global mean and patterned components, which are here termed as the global mean ΔQ_{net} effect and the patterned ΔQ_{net} effect, respectively. As climate warming continues, the deep ocean comes into closer balance with the atmosphere, diminishing the global-mean ΔQ_{net}, and as a result, the cooling effect due to the global mean ΔQ_{net} is expected to decrease over time (see Fig. 2b). In contrast, the patterned ΔQ_{net} effect is much less well constrained in terms of its sign, magnitude, and evolution.

Figure 8 shows the global mean ΔQ_{net} effect and the patterned ΔQ_{net} effect based on our SOM simulations. The mean ΔQ_{net} effect acts to cool the global climate (Fig. 8a), and its spatial structure is very similar to the direct CO_2 effect in the absence of Q_{net} changes (Fig. 4a; $r = -0.87$). This is not surprising given the largely uniform CO_2 radiative forcing in space. The patterned ΔQ_{net} effect also acts to cool the global climate except for the equatorial band where very weak warming is observed (Fig. 8c), which is striking because the global average of the patterned ΔQ_{net} is zero by construction. It suggests that the spatial variations of ΔQ_{net} can effectively rectify on the mean climate and induce a net global cooling. These results are consistent with previous idealized modeling

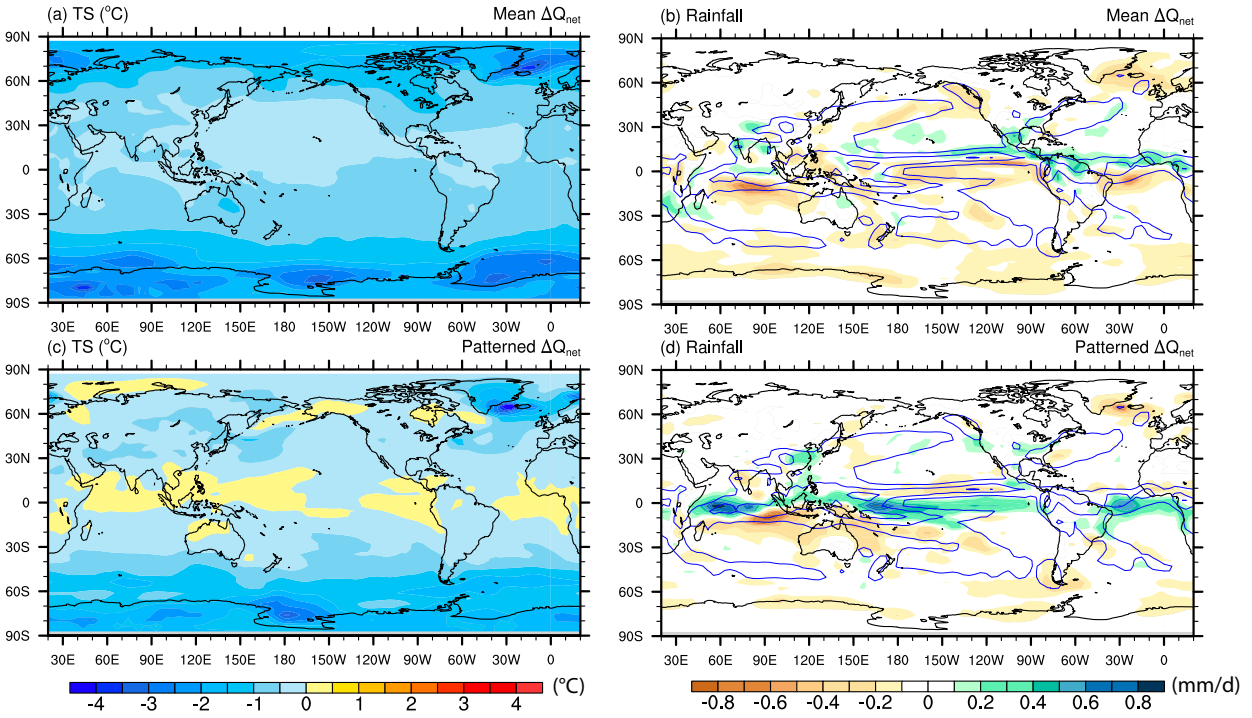

FIG. 8. Changes in annual-mean (left) surface temperature (°C) and (right) precipitation (mm day^{-1}) associated with (a),(b) the global mean ΔQ_{net} effect (SOM_Cx2GM − SOM_Cx2REF), and (c),(d) the patterned ΔQ_{net} effect (SOM_Cx2SP − SOM_Cx2REF). In the rainfall panels, blue contours are for annual-mean climatological rainfall in SOM_CTL with an interval of 3 mm day^{-1}.

studies arguing that the effect of ocean heat uptake on GMST depends on the meridional forcing structure (Alexeev et al. 2005; Rose et al. 2014; Kang and Xie 2014). In our case, the patterned ΔQ_{net} effect on GMST reaches about a half of the mean ΔQ_{net} effect (−0.40° vs −0.83°C, respectively) for the time period we are investigating (i.e., 4–5 decades after the CO_2 doubling). The spatial pattern of surface temperature change associated with the mean ΔQ_{net} effect resembles that associated with the patterned ΔQ_{net} effect, even though the absolute values are different; the pattern correlation between the two is 0.73 (Figs. 8a,c).

The meridional structure of the ocean heat uptake–induced, zonal-mean rainfall changes are primarily shaped by the patterned ΔQ_{net} effect (Fig. 9b). The sharp rainfall increase in the equatorial band comes entirely from the patterned ΔQ_{net} effect and is found over all three ocean basins (Fig. 8d), partly compensated by the global mean ΔQ_{net} effect (Fig. 8b). This is because the ΔQ_{net} pattern features largely positive values in the high latitudes and weakly negative values at the equator, leading to a global-scale cooling but significantly weaker near the equator (Fig. 9a). As we will demonstrate further in section 4d, this effect directly contributes to the equatorially enhanced sea surface warming in the net response to CO_2 increase (Fig. 3a) and therefore leads to an equatorially enhanced rainfall increase. The global mean ΔQ_{net} acts to reduce the rainfall globally and slightly push the ITCZ northward in the tropics (Figs. 8b and 9b).

d. Tropical rainfall change pattern

Beyond the zonal-mean change, tropical rainfall response has rich regional features in its zonal variations (Fig. 10). Previous studies suggest that tropical rainfall change pattern under global warming is largely controlled by the SST change pattern (e.g., Xie et al. 2010). Following those studies, in Fig. 10 we also plot the relative SST, which is defined as the difference between local SST and the tropical-mean SST averaged within 20°S–20°N. In all our DOM and SOM simulations, we find consistent results that a positive (negative) relative SST change is typically associated with a rainfall increase (decrease), with interesting notable exceptions near the equator and the date line in Figs. 10b and 10c.

Forced by the DOM ΔQ_{net}, the SOM simulations can reasonably reproduce the tropical relative SST change pattern and thus the tropical rainfall change pattern in the DOM (cf. Figs. 10a,b). Over the tropical oceans, both the direct CO_2 effect and the ΔQ_{net} effect turn out to be critical in shaping the rainfall change pattern (Figs. 10c,d). Over the Indian Ocean, the generally enhanced rainfall is mostly due to the CO_2-induced local warming, while the northward shift of the rainfall center is dominated by the ΔQ_{net} effect. Over the tropical Atlantic, the direct CO_2 effect induces a rainfall reduction due to the relatively weak warming near the equator, but this is largely cancelled out by the rainfall enhancement induced by the ΔQ_{net} effect. Over the tropical Pacific, rainfall change is dominated by an equatorial increase and an off-equatorial decrease on either side, with both the CO_2 and

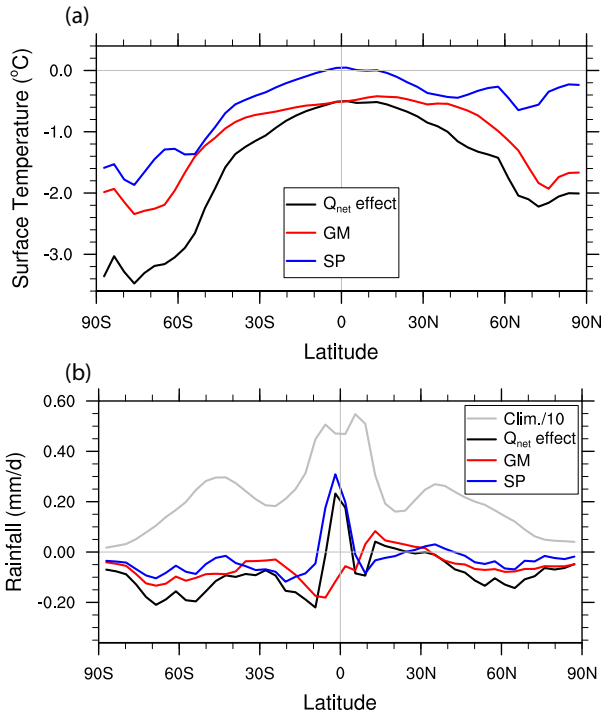

FIG. 9. Zonal-mean changes in annual-mean (a) surface temperature (°C) and (b) precipitation (mm day^{-1}) in different simulations. Here the Q_{net} effect is SOM_Cx2 − SOM_Cx2REF; GM is SOM_Cx2GM − SOM_Cx2REF, the global mean ΔQ_{net} effect; and SP is SOM_Cx2SP − SOM_Cx2REF, the patterned ΔQ_{net} effect. In (b), the gray line is for the climatological annual-mean precipitation divided by 10.

ΔQ_{net} effects contributing to this pattern. The direct CO_2 effect features an equatorial warming in the eastern equatorial Pacific and a negative relative SST on both sides. Over tropical continents, rainfall changes come almost entirely from the direct CO_2 effect, while the SST changes associated with the ΔQ_{net} effect only plays a minor role.

For the ΔQ_{net} effect, one common feature to the three tropical oceans is the rainfall increase along the equatorial band (Fig. 10d), together yielding a sharp, equatorially enhanced rainfall seen in the zonal-mean plot (Fig. 5b). As we mentioned earlier, this is an inherent feature determined by the spatial structure of ΔQ_{net}. This mechanism is confirmed by the fact that the feature of equatorial rainfall increase comes entirely from the patterned ΔQ_{net} effect (Fig. 10h), while the mean ΔQ_{net} effect acts to push the ITCZ northward with mild rainfall changes in the equatorial band (Fig. 10f). The experiments with a latitudinal decomposition of ΔQ_{net} further suggest that the weakly negative ΔQ_{net} at the equator, in contrast with the mostly positive ΔQ_{net} elsewhere, plays a dominant role in giving rise to the positive relative SST and the increased rainfall along the equatorial band in all three oceans (Fig. 10g).

The seemingly similar, zonal-mean equatorial rainfall enhancement seen in the direct CO_2 effect (Fig. 11), however, comes mainly from the land rainfall increase over central Africa, western South America, and the Maritime Continent (Fig. 10c). Over the oceans, the direct CO_2 effect actually induce a rainfall reduction in both the equatorial Atlantic and Indian Ocean and a slight rainfall increase in the central-eastern equatorial Pacific, both consistent with the local relative SST changes. Our results imply that zonal-mean rainfall changes under global warming result from delicate partitioning between ocean and land components, and among the three ocean basins.

Our decomposition of the ΔQ_{net} effect reveals how regional ΔQ_{net} forcing influences the tropical rainfall changes. The southern ocean ΔQ_{net} generates a strong interhemispheric asymmetry of SST changes in all three tropical oceans, pushing the ITCZ northward, and the impact is particularly strong for the Indian Ocean (Fig. 10i). The northern ocean ΔQ_{net} does the opposite, acting to push the ITCZ southward at all longitudes, but the magnitudes of relative SST and rainfall changes are considerably smaller (Fig. 10e; Kang et al. 2020). The general patterns of rainfall changes look much alike for the two extratropical ΔQ_{net} effects ($r = -0.74$ for rainfall and $r = -0.76$ for relative SST within 20°S–20°N), suggesting an intrinsic, interhemispheric mode of tropical rainfall response to extratropical forcing. A further decomposition of the northern ocean ΔQ_{net} suggests that the North Atlantic ΔQ_{net} plays a dominant role, although the contributions from other ocean basins are not negligible (not shown). The response to the tropical ocean ΔQ_{net} resembles that to the northern oceans' ΔQ_{net} ($r = 0.47$ for rainfall and $r = 0.61$ for relative SST within 20°S–20°N) (Fig. 10g). It includes a southward shift of ITCZ in the tropical Pacific and Atlantic and a zonal-dipole structure in the Indian Ocean, both consistent with the underlying relative SST change patterns; in addition, a signal of equatorial rainfall enhancement is found in all three ocean basins (Fig. 10g).

5. Summary and discussion

In this study, we have used a SOM as a diagnostic modeling tool to better understand the surface warming pattern formation under transient climate change, with a particular focus on the role of ΔQ_{net} (i.e., ocean surface heat uptake). We find that SOM simulations reproduce quite well the DOM-simulated global warming pattern and tropical rainfall changes, when forced with the DOM ΔQ_{net}. We emphasize that a critical step to reproducing the DOM climate in the SOM is to retain the global-mean ΔQ_{net} that is diagnosed from the DOM. This then allows us to transform an initial-value problem for transient climate change to a boundary-value problem, allowing us to conduct further attribution to a set of constituent forcing factors. The direct CO_2 effect in the absence of Q_{net} changes leads to a substantial global warming, partially compensated by the cooling effect of ΔQ_{net}.

The direct CO_2 warming effect is accompanied by a considerable polar amplification, due primarily to the latitudinal dependence of climate feedback (e.g., Alexeev et al. 2005; Taylor et al. 2013; Armour et al. 2013; Park et al. 2018; Stuecker et al. 2018; Goosse et al. 2018). The ΔQ_{net} cooling

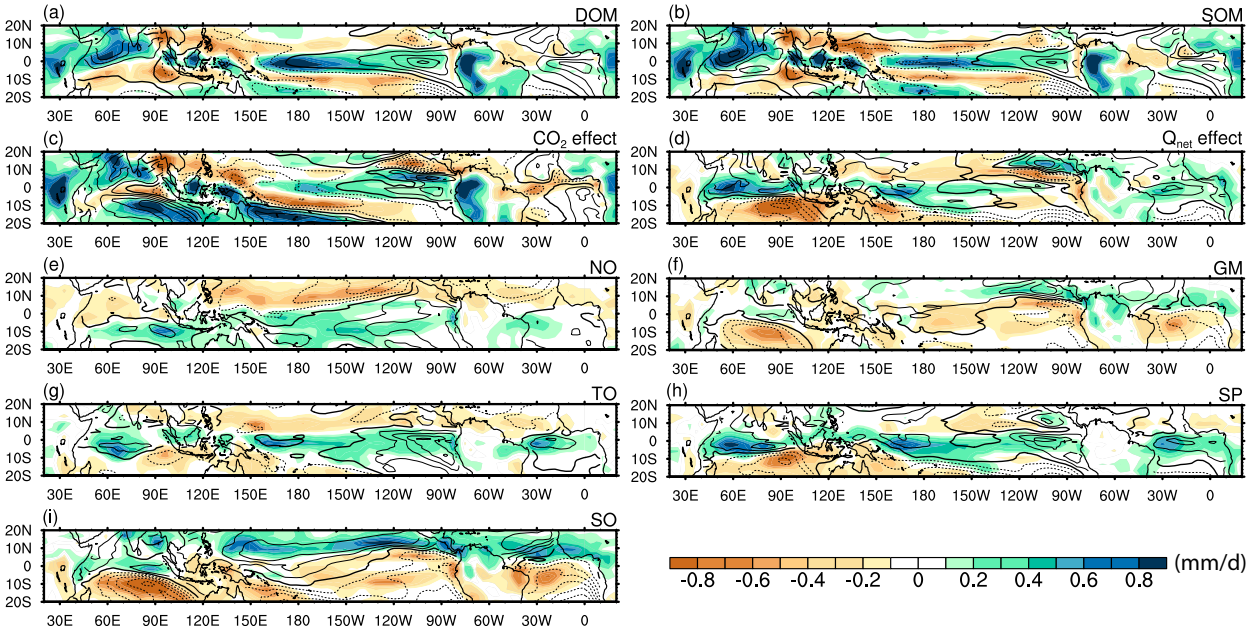

FIG. 10. Changes in tropical rainfall (colors; mm day^{-1}) and relative SST (contours; °C) in different simulations as indicated at the top-right corner. Relative SST is defined as the difference between local SST and tropical-mean SST averaged within 20°S–20°N; thick solid, thin solid, and dashed are for zero, positive, and negative values, respectively, with a contour interval of 0.1°C. Here DOM is DOM_Cx2 − DOM_CTL, SOM is SOM_Cx2 − SOM_CTL, the CO_2 effect is SOM_Cx2REF − SOM_CTL, the Q_{net} effect is SOM_Cx2 − SOM_Cx2-REF, NO is SOM_Cx2NO − SOM_Cx2REF, TO is SOM_Cx2TO − SOM_Cx2REF, SO is SOM_Cx2SO − SOM_Cx2REF, GM is SOM_Cx2GM − SOM_Cx2REF, and SP is SOM_Cx2SP − SOM_Cx2REF.

effect exhibits a similar but stronger polar amplification, because the strongest signals of positive ΔQ_{net} (i.e., downward into the ocean) are confined over the high latitudes in both hemispheres. The net impact of the two leads to a polar amplification of surface warming weaker than that for the CO_2 warming effect alone. Our results suggest that the inter-model spread of polar amplification previously identified (Bindoff et al. 2013; Smith et al. 2019) may potentially be caused by the different meridional structure of ΔQ_{net}, in addition to the role of radiative forcing and climate feedback (Bonan et al. 2018).

In our transient experiments, polar amplification is asymmetric between the two hemispheres, as has been observed in the historical period and also commonly simulated in climate models (e.g., Manabe et al. 1990; Bindoff et al. 2013; Singh et al. 2017; Smith et al. 2019). For the direct CO_2 effect, Antarctic amplification has comparable magnitude to Arctic amplification, suggesting that the coupled atmosphere–ocean mixed layer response would lead to symmetric polar amplification in our model. However, the ΔQ_{net} cooling effect is much more polar amplified in the Southern Hemisphere, due mainly to the strong ocean heat uptake that occurs in the Southern Ocean (Fig. 5a). As a result, in the net warming response, polar amplification is more muted over the Antarctica than the Arctic due to the stronger cancellation between the two effects. These results imply that the distinct behaviors of polar amplification between the Arctic and the Antarctic is perhaps inherently linked to the ocean surface heat uptake pattern. Our finding on the potential role of Southern Ocean heat uptake in reducing Antarctic amplification is broadly consistent with previous modeling studies (e.g., Manabe et al. 1990; Marshall et al. 2014, 2015; Armour et al. 2016). We note that the regional peaks of ΔQ_{net} in the Southern Ocean and the subpolar North Atlantic may result from independent dynamical mechanisms, which remain under debate (e.g., Marshall et al. 2015; Armour et al. 2016; Shi et al. 2018; Hu et al. 2020), and the degree of polar amplification and hemispheric symmetry in surface temperature changes may vary in other models or at different stages of transient warming.

Another salient feature of simulated global warming response to greenhouse gas increase is the equatorially enhanced warming, most pronounced in the tropical Pacific (Fig. 10a; also see Liu et al. 2005; Zhou et al. 2019; Heede et al. 2020). We find that this is an intrinsic feature associated with the ΔQ_{net} effect. Since ΔQ_{net} is strongly positive in the high latitudes and weakly negative at the equator (Fig. 2c), its resultant global cooling maximizes in the high latitudes and minimizes at the equator for all three ocean basins, particularly evident in the Atlantic and Indian Oceans (Fig. 4c). For the direct CO_2 effect, the SST response is controlled purely by thermodynamic effects, and the three equatorial oceans exhibit different behaviors. Since the eastern equatorial Pacific is characterized by a strong cold tongue and a high surface relative humidity, it needs to warm more to compensate for the CO_2-induced radiative forcing (Liu et al. 2005; Xie et al. 2010); however, this effect might have been overestimated in the model because climate models generally suffer from a positive relative humidity bias over the Pacific cold

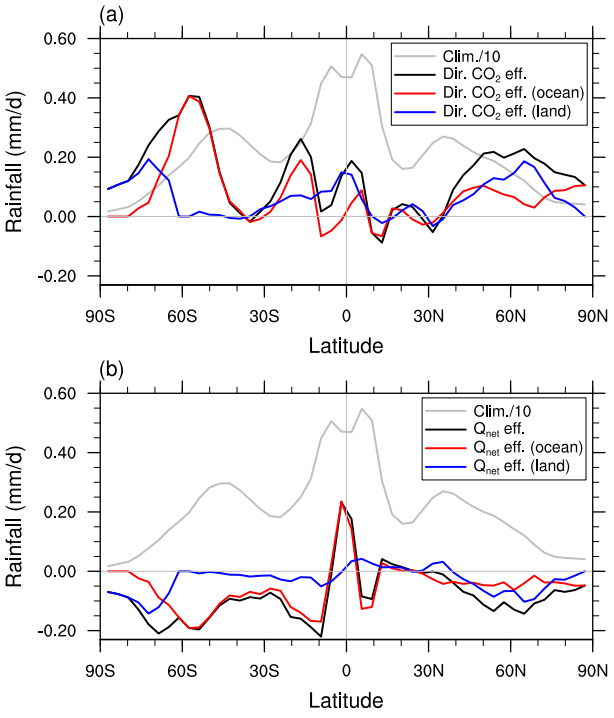

FIG. 11. Land–ocean decomposition of zonal-mean changes in annual-mean precipitation (mm day^{-1}) for (a) the direct CO_2 effect and (b) the ΔQ_{net} effect. Red (blue) lines are derived using the zonal average of rainfall rate after replacing all the land (ocean) values with zero. The black line equals the addition of the red and blue lines by design. In both panels, the gray line is for the climatological annual-mean precipitation divided by 10.

tongue (Seager et al. 2019). The equatorial cold tongue is weaker in the Atlantic especially in the models and absent in the Indian Ocean, and in fact, in those two ocean basins, weaker warming is observed near the equatorial band than over the subtropical ocean. In summary, the direct CO_2 effect and the ΔQ_{net} effect act in the same direction and give rise to a pronounced equatorial enhanced warming in the Pacific in terms of relative SST, but they largely compensate in the Atlantic and Indian Ocean in terms of warming structure (Figs. 10c,d).

Tropical rainfall change is similarly enhanced in the equatorial band, shaped in part by the SST warming pattern. The ΔQ_{net} effect, mainly its spatially varying component, acts to increase the equatorial rainfall over all three ocean basins, as a result of the equatorially enhanced warming. The direct CO_2 effect leads to competing rainfall changes among the equatorial oceans, an increase in the central-eastern Pacific but a reduction in the Indo-western Pacific and the Atlantic, controlled by the relative SST pattern; however, it causes consistent increase in rainfall over the tropical continents, including western South America, central Africa, and the Maritime Continent. As a result, both the direct CO_2 effect and the ΔQ_{net} effect lead to an equatorial enhancement of zonal-mean rainfall, but it is important to realize that they result from different physical mechanisms.

No robust ITCZ shift can be detected in the zonal-mean rainfall response to CO_2 doubling in our DOM. The southern ocean ΔQ_{net} induces a significant Southern Hemisphere cooling, pushing the ITCZ northward in all three tropical oceans, but this is largely cancelled out by the northern ocean ΔQ_{net} effect. The tropical ocean ΔQ_{net} effect opposes the strong southern ocean ΔQ_{net} effect, pushing the ITCZ southward. This is consistent with the previous finding that an extratropical heat source can potentially influence the Ekman heat transport in the tropical oceans, inducing a negative feedback that damps the response to extratropical forcing (Kay et al. 2016; Green and Marshall 2017; Schneider 2017; Kang et al. 2018). In addition, the tropical ocean ΔQ_{net} results in an equatorially enhanced rainfall in all three ocean basins. The northern ocean ΔQ_{net}-induced cooling effect leads to a southward shift of ITCZ, further compensating for the southern ocean ΔQ_{net} effect. As a result of the strong compensation, the global ΔQ_{net} has little net impact on the ITCZ shift in the tropical Atlantic and Pacific, except for the Indian Ocean that is dominated by the southern ocean ΔQ_{net} effect. For the direct CO_2 effect, there is no significant signal of ITCZ shift, given the similar warming magnitude in the two hemispheres.

Decomposing the ΔQ_{net} effect into its global mean and pattern components provides us additional insights to understanding the global warming pattern formation and evolution. The global mean ΔQ_{net} effect acts similarly to the direct CO_2 effect but with an opposite sign. The patterned ΔQ_{net} effect contributes significantly to a global-scale cooling, although the ΔQ_{net} is averaged to zero globally. Those results are consistent with previous studies using idealized simulations to argue that the effect of ocean heat uptake on global mean temperature depends on the meridional forcing structure (Alexeev et al. 2005; Rose et al. 2014; Kang and Xie 2014). See Rose and Rayborn (2016) for a recent review.

Our study extends the SOM framework to understand the transient global warming pattern and rainfall change from the ΔQ_{net} distribution. This is complementary to our recent work that focuses on the oceanic mechanism for ΔQ_{net} (Hu et al. 2020). Together, these results confirm the importance of ocean–atmosphere coupling in shaping the global warming pattern, and the critical role of ΔQ_{net} or ocean heat uptake suggested in the existing literature. The detailed physical mechanisms underlying the coupling of atmospheric and oceanic processes through surface heat, momentum, and freshwater fluxes require further investigations (Fig. 1). The relative roles of greenhouse gases and aerosols in shaping the historical and future warming patterns through ocean–atmosphere interaction also need to be further explored.

Acknowledgments. We acknowledge computational support from the NSF/NCAR Cheyenne Supercomputing Center. Discussions with Richard Seager and Mark Cane are gratefully acknowledged. We thank Clara Deser and two anonymous reviewers for their constructive comments that have greatly improved the manuscript. S. Hu was supported by the Scripps Institutional and Lamont-Doherty Earth Observatory Postdoctoral Fellowships, S.-P. Xie by the U.S.

National Science Foundation (AGS-1934392), and S. Kang by the National Research Foundation of Korea (NRF) funded by the South Korean government (MSIT) (Grant 2020R1A2C2101503).

Data availability statement. The model output from all the simulations conducted in this study are available at https://doi.org/10.5281/zenodo.5717333.

REFERENCES

Alexeev, V. A., P. L. Langen, and J. R. Bates, 2005: Polar amplification of surface warming on an aquaplanet in "ghost forcing" experiments without sea ice feedbacks. *Climate Dyn.*, **24**, 655–666, https://doi.org/10.1007/s00382-005-0018-3.

Armour, K. C., C. M. Bitz, and G. H. Roe, 2013: Time-varying climate sensitivity from regional feedbacks. *J. Climate*, **26**, 4518–4534, https://doi.org/10.1175/JCLI-D-12-00544.1.

——, J. Marshall, J. R. Scott, A. Donohoe, and E. R. Newsom, 2016: Southern Ocean warming delayed by circumpolar upwelling and equatorward transport. *Nat. Geosci.*, **9**, 549–554, https://doi.org/10.1038/ngeo2731.

Back, L. E., and C. S. Bretherton, 2009: On the relationship between SST gradients, boundary layer winds, and convergence over the tropical oceans. *J. Climate*, **22**, 4182–4196, https://doi.org/10.1175/2009JCLI2392.1.

Banks, H. T., and J. M. Gregory, 2006: Mechanisms of ocean heat uptake in a coupled climate model and the implications for tracer based predictions of ocean heat uptake. *Geophys. Res. Lett.*, **33**, L07608, https://doi.org/10.1029/2005GL025352.

Bindoff, N. L., and Coauthors, 2013: Detection and attribution of climate change: From global to regional. *Climate Change 2013: The Physical Science Basis*, T. F. Stocker, Eds., Cambridge University Press, 867–952.

Bischoff, T., and T. Schneider, 2014: Energetic constraints on the position of the intertropical convergence zone. *J. Climate*, **27**, 4937–4951, https://doi.org/10.1175/JCLI-D-13-00650.1.

Bitz, C. M., K. M. Shell, P. R. Gent, D. A. Bailey, G. Danabasoglu, K. C. Armour, M. M. Holland, and J. T. Kiehl, 2012: Climate sensitivity of the Community Climate System Model, version 4. *J. Climate*, **25**, 3053–3070, https://doi.org/10.1175/JCLI-D-11-00290.1.

Bonan, D. B., K. C. Armour, G. H. Roe, N. Siler, and N. Feldl, 2018: Sources of uncertainty in the meridional pattern of climate change. *Geophys. Res. Lett.*, **45**, 9131–9140, https://doi.org/10.1029/2018GL079429.

Broccoli, A. J., K. A. Dahl, and R. J. Stouffer, 2006: Response of the ITCZ to Northern Hemisphere cooling. *Geophys. Res. Lett.*, **33**, L01702, https://doi.org/10.1029/2005GL024546.

Deser, C., and Coauthors, 2020: Isolating the evolving contributions of anthropogenic aerosols and greenhouse gases: A new CESM1 large ensemble community resource. *J. Climate*, **33**, 7835–7858, https://doi.org/10.1175/JCLI-D-20-0123.1.

Dong, B., J. M. Gregory, and R. T. Sutton, 2009: Understanding land–sea warming contrast in response to increasing greenhouse gases. Part I: Transient adjustment. *J. Climate*, **22**, 3079–3097, https://doi.org/10.1175/2009JCLI2652.1.

Dong, Y., C. Proistosescu, K. C. Armour, and D. S. Battisti, 2019: Attributing historical and future evolution of radiative feedbacks to regional warming patterns using a Green's function approach: The preeminence of the western Pacific. *J. Climate*, **32**, 5471–5491, https://doi.org/10.1175/JCLI-D-18-0843.1.

——, K. C. Armour, M. D. Zelinka, C. Proistosescu, D. S. Battisti, C. Zhou, and T. Andrews, 2020: Intermodel spread in the pattern effect and its contribution to climate sensitivity in CMIP5 and CMIP6 models. *J. Climate*, **33**, 7755–7775, https://doi.org/10.1175/JCLI-D-19-1011.1.

Drijfhout, S., G. J. Van Oldenborgh, and A. Cimatoribus, 2012: Is a decline of AMOC causing the warming hole above the North Atlantic in observed and modeled warming patterns? *J. Climate*, **25**, 8373–8379, https://doi.org/10.1175/JCLI-D-12-00490.1.

Duffy, M. L., P. A. O'Gorman, and L. E. Back, 2020: Importance of Laplacian of low-level warming for the response of precipitation to climate change over tropical oceans. *J. Climate*, **33**, 4403–4417, https://doi.org/10.1175/JCLI-D-19-0365.1.

England, M. R., L. M. Polvani, L. Sun, and C. Deser, 2020: Tropical climate responses to projected Arctic and Antarctic sea-ice loss. *Nat. Geosci.*, **13**, 275–281, https://doi.org/10.1038/s41561-020-0546-9.

Garuba, O. A., J. Lu, F. Liu, and H. A. Singh, 2018: The active role of the ocean in the temporal evolution of climate sensitivity. *Geophys. Res. Lett.*, **45**, 306–315, https://doi.org/10.1002/2017GL075633.

Gent, P. R., and Coauthors, 2011: The Community Climate System Model version 4. *J. Climate*, **24**, 4973–4991, https://doi.org/10.1175/2011JCLI4083.1.

Gervais, M., J. Shaman, and Y. Kushnir, 2019: Impacts of the North Atlantic warming hole in future climate projections: Mean atmospheric circulation and the North Atlantic jet. *J. Climate*, **32**, 2673–2689, https://doi.org/10.1175/JCLI-D-18-0647.1.

Goosse, H., and Coauthors, 2018: Quantifying climate feedbacks in polar regions. *Nat. Commun.*, **9**, 1919, https://doi.org/10.1038/s41467-018-04173-0.

Green, B., and J. Marshall, 2017: Coupling of trade winds with ocean circulation damps ITCZ shifts. *J. Climate*, **30**, 4395–4411, https://doi.org/10.1175/JCLI-D-16-0818.1.

Haugstad, A. D., K. C. Armour, D. S. Battisti, and B. E. J. Rose, 2017: Relative roles of surface temperature and climate forcing patterns in the inconstancy of radiative feedbacks. *Geophys. Res. Lett.*, **44**, 7455–7463, https://doi.org/10.1002/2017GL074372.

He, J., C. Deser, and B. J. Soden, 2017: Atmospheric and oceanic origins of tropical precipitation variability. *J. Climate*, **30**, 3197–3217, https://doi.org/10.1175/JCLI-D-16-0714.1.

Heede, U. K., A. V. Fedorov, and N. J. Burls, 2020: Time scales and mechanisms for the tropical Pacific response to global warming: A tug of war between the ocean thermostat and weaker Walker. *J. Climate*, **33**, 6101–6118, https://doi.org/10.1175/JCLI-D-19-0690.1.

Held, I. M., M. Winton, K. Takahashi, T. Delworth, F. Zeng, and G. K. Vallis, 2010: Probing the fast and slow components of global warming by returning abruptly to preindustrial forcing. *J. Climate*, **23**, 2418–2427, https://doi.org/10.1175/2009JCLI3466.1.

Hill, S. A., N. J. Burls, A. Fedorov, and T. M. Merlis, 2020: Symmetric and antisymmetric components of polar-amplified warming. https://arxiv.org/abs/2012.09228.

Hu, S., and A. V. Fedorov, 2020: Indian Ocean warming as a driver of the North Atlantic warming hole. *Nat. Commun.*, **11**, 4785, https://doi.org/10.1038/s41467-020-18522-5.

——, S.-P. Xie, and W. Liu, 2020: Global pattern formation of net ocean surface heat flux response to greenhouse warming. *J. Climate*, **33**, 7503–7522, https://doi.org/10.1175/JCLI-D-19-0642.1.

Huang, Y., Y. Xia, and X. Tan, 2017: On the pattern of CO_2 radiative forcing and poleward energy transport. *J. Geophys. Res. Atmos.*, **122**, 10 578–10 593, https://doi.org/10.1002/2017JD027221.

Huber, M. B., and L. Zanna, 2017: Drivers of uncertainty in simulated ocean circulation and heat uptake. *Geophys. Res. Lett.*, **44**, 1402–1413, https://doi.org/10.1002/2016GL071587.

Hwang, Y. T., and D. M. Frierson, 2013: Link between the double-Intertropical Convergence Zone problem and cloud biases over the Southern Ocean. *Proc. Natl. Acad. Sci. USA*, **110**, 4935–4940, https://doi.org/10.1073/pnas.1213302110.

——, S.-P. Xie, C. Deser, and S. M. Kang, 2017: Connecting tropical climate change with Southern Ocean heat uptake. *Geophys. Res. Lett.*, **44**, 9449–9457, https://doi.org/10.1002/2017GL074972.

Kang, S. M., and S.-P. Xie, 2014: Dependence of climate response on meridional structure of external thermal forcing. *J. Climate*, **27**, 5593–5600, https://doi.org/10.1175/JCLI-D-13-00622.1.

——, I. M. Held, D. M. Frierson, and M. Zhao, 2008: The response of the ITCZ to extratropical thermal forcing: Idealized slab-ocean experiments with a GCM. *J. Climate*, **21**, 3521–3532, https://doi.org/10.1175/2007JCLI2146.1.

——, D. M. Frierson, and I. M. Held, 2009: The tropical response to extratropical thermal forcing in an idealized GCM: The importance of radiative feedbacks and convective parameterization. *J. Atmos. Sci.*, **66**, 2812–2827, https://doi.org/10.1175/2009JAS2924.1.

——, K. Park, F.-F. Jin, and M. F. Stuecker, 2017: Common warming pattern emerges irrespective of forcing location. *J. Adv. Model. Earth Syst.*, **9**, 2413–2424, https://doi.org/10.1002/2017MS001083.

——, Y. Shin, and S.-P. Xie, 2018: Extratropical forcing and tropical rainfall distribution: Energetics framework and ocean Ekman advection. *npj Climate Atmos. Sci.*, **1**, 20172, https://doi.org/10.1038/s41612-017-0004-6.

——, S.-P. Xie, Y. Shin, H. Kim, Y.-T. Hwang, M. F. Stuecker, B. Xiang, and M. Hawcroft, 2020: Walker circulation response to extratropical radiative forcing. *Sci. Adv.*, **6**, eabd3021, https://doi.org/10.1126/sciadv.abd3021.

Kay, J. E., and Coauthors, 2015: The Community Earth System Model (CESM) large ensemble project: A community resource for studying climate change in the presence of internal climate variability. *Bull. Amer. Meteor. Soc.*, **96**, 1333–1349, https://doi.org/10.1175/BAMS-D-13-00255.1.

——, C. Wall, V. Yettella, B. Medeiros, C. Hannay, P. Caldwell, and C. Bitz, 2016: Global climate impacts of fixing the Southern Ocean shortwave radiation bias in the Community Earth System Model (CESM). *J. Climate*, **29**, 4617–4636, https://doi.org/10.1175/JCLI-D-15-0358.1.

Lau, W. K. M., H. T. Wu, and K. M. Kim, 2013: A canonical response of precipitation characteristics to global warming from CMIP5 models. *Geophys. Res. Lett.*, **40**, 3163–3169, https://doi.org/10.1002/grl.50420.

Lin, Y. J., Y. T. Hwang, J. Lu, F. Liu, and B. E. Rose, 2021: The dominant contribution of Southern Ocean heat uptake to time-evolving radiative feedback in CESM. *Geophys. Res. Lett.*, **48**, e2021GL093302, https://doi.org/10.1029/2021GL093302.

Liu, F., J. Lu, O. Garuba, L. R. Leung, Y. Luo, and X. Wan, 2018a: Sensitivity of surface temperature to oceanic forcing via *q*-flux Green's function experiments. Part I: Linear response function. *J. Climate*, **31**, 3625–3641, https://doi.org/10.1175/JCLI-D-17-0462.1.

——, ——, ——, Y. Huang, L. R. Leung, B. E. Harrop, and Y. Luo, 2018b: Sensitivity of surface temperature to oceanic forcing via *q*-flux Green's function experiments. Part II: Feedback decomposition and polar amplification. *J. Climate*, **31**, 6745–6761, https://doi.org/10.1175/JCLI-D-18-0042.1.

Liu, Z., S. Vavrus, F. He, N. Wen, and Y. Zhong, 2005: Rethinking tropical ocean response to global warming: The enhanced equatorial warming. *J. Climate*, **18**, 4684–4700, https://doi.org/10.1175/JCLI3579.1.

Manabe, S., K. Bryan, and M. J. Spelman, 1990: Transient response of a global ocean–atmosphere model to a doubling of atmospheric carbon dioxide. *J. Phys. Oceanogr.*, **20**, 722–749, https://doi.org/10.1175/1520-0485(1990)020<0722:TROAGO>2.0.CO;2.

Marshall, J., K. C. Armour, J. R. Scott, Y. Kostov, U. Hausmann, D. Ferreira, T. G. Shepherd, and C. M. Bitz, 2014: The ocean's role in polar climate change: Asymmetric Arctic and Antarctic responses to greenhouse gas and ozone forcing. *Philos. Trans. Roy. Soc.*, **372A**, 20130040, https://doi.org/10.1098/rsta.2013.0040.

——, J. R. Scott, K. C. Armour, J. M. Campin, M. Kelley, and A. Romanou, 2015: The ocean's role in the transient response of climate to abrupt greenhouse gas forcing. *Climate Dyn.*, **44**, 2287–2299, https://doi.org/10.1007/s00382-014-2308-0.

Mitchell, J. F. B., R. A. Davis, W. A. Ingram, and C. A. Senior, 1995: On surface temperature, greenhouse gases, and aerosols: Models and observations. *J. Climate*, **8**, 2364–2386, https://doi.org/10.1175/1520-0442(1995)008<2364:OSTGGA>2.0.CO;2.

Neale, R. B., Coauthors, 2010: Description of the NCAR Community Atmosphere Model (CAM 4.0). NCAR Tech. Note NCAR/TN-485+STR, 224 pp.

Park, K., S.-M. Kang, D. Kim, M. F. Stuecker, and F.-F. Jin, 2018: Contrasting local and remote impacts of surface heating on polar warming and amplification. *J. Climate*, **31**, 3155–3166, https://doi.org/10.1175/JCLI-D-17-0600.1.

Rose, B. E., and L. Rayborn, 2016: The effects of ocean heat uptake on transient climate sensitivity. *Curr. Climate Change Rep.*, **2**, 190–201, https://doi.org/10.1007/s40641-016-0048-4.

——, K. C. Armour, D. S. Battisti, N. Feldl, and D. D. Koll, 2014: The dependence of transient climate sensitivity and radiative feedbacks on the spatial pattern of ocean heat uptake. *Geophys. Res. Lett.*, **41**, 1071–1078, https://doi.org/10.1002/2013GL058955.

Rugenstein, M. A., K. Caldeira, and R. Knutti, 2016: Dependence of global radiative feedbacks on evolving patterns of surface heat fluxes. *Geophys. Res. Lett.*, **43**, 9877–9885, https://doi.org/10.1002/2016GL070907.

Schneider, T., 2017: Feedback of atmosphere–ocean coupling on shifts of the Intertropical Convergence Zone. *Geophys. Res. Lett.*, **44**, 11 644–11 654, https://doi.org/10.1002/2017GL075817.

Seager, R., M. Cane, N. Henderson, D. E. Lee, R. Abernathey, and H. Zhang, 2019: Strengthening tropical Pacific zonal sea surface temperature gradient consistent with rising greenhouse gases. *Nat. Climate Change*, **9**, 517–522, https://doi.org/10.1038/s41558-019-0505-x.

Shi, J.-R., S.-P. Xie, and L. D. Talley, 2018: Evolving relative importance of the Southern Ocean and North Atlantic in anthropogenic ocean heat uptake. *J. Climate*, **31**, 7459–7479, https://doi.org/10.1175/JCLI-D-18-0170.1.

Shindell, D., and G. Faluvegi, 2009: Climate response to regional radiative forcing during the twentieth century. *Nat. Geosci.*, **2**, 294–300, https://doi.org/10.1038/ngeo473.

Singh, H. A., P. J. Rasch, and B. E. J. Rose, 2017: Increased ocean heat convergence into the high latitudes with CO_2 doubling enhances polar-amplified warming. *Geophys. Res. Lett.*, **44**, 10 583–10 591, https://doi.org/10.1002/2017GL074561.

——, O. A. Garuba, and P. J. Rasch, 2018: How asymmetries between Arctic and Antarctic climate sensitivity are modified by the ocean. *Geophys. Res. Lett.*, **45**, 13031–13040, https://doi.org/10.1029/2018GL079023.

Smith, D. M., and Coauthors, 2019: The Polar Amplification Model Intercomparison Project (PAMIP) contribution to CMIP6: Investigating the causes and consequences of polar amplification. *Geosci. Model Dev.*, **12**, 1139–1164, https://doi.org/10.5194/gmd-12-1139-2019.

Smith, R. D., and Coauthors, 2010: The Parallel Ocean Program (POP) reference manual. Tech. Rep. LAUR-10-01853, Los Alamos National Laboratory, 141 pp.

Stuecker, M. F., and Coauthors, 2018: Polar amplification dominated by local forcing and feedbacks. *Nat. Climate Change*, **8**, 1076–1081, https://doi.org/10.1038/s41558-018-0339-y.

——, and Coauthors, 2020: Strong remote control of future equatorial warming by off-equatorial forcing. *Nat. Climate Change*, **10**, 124–129, https://doi.org/10.1038/s41558-019-0667-6.

Taylor, P. C., M. Cai, A. Hu, J. Meehl, W. Washington, and G. J. Zhang, 2013: A decomposition of feedback contributions to polar warming amplification. *J. Climate*, **26**, 7023–7043, https://doi.org/10.1175/JCLI-D-12-00696.1.

Tomas, R. A., C. Deser, and L. Sun, 2016: The role of ocean heat transport in the global climate response to projected Arctic sea ice loss. *J. Climate*, **29**, 6841–6859, https://doi.org/10.1175/JCLI-D-15-0651.1.

Wang, H., S.-P. Xie, and Q. Liu, 2016: Comparison of climate response to anthropogenic aerosol versus greenhouse gas forcing: Distinct patterns. *J. Climate*, **29**, 5175–5188, https://doi.org/10.1175/JCLI-D-16-0106.1.

Wang, K., C. Deser, L. Sun, and R. A. Tomas, 2018: Fast response of the tropics to an abrupt loss of Arctic sea ice via ocean dynamics. *Geophys. Res. Lett.*, **45**, 4264–4272, https://doi.org/10.1029/2018GL077325.

Winton, M., K. Takahashi, and I. M. Held, 2010: Importance of ocean heat uptake efficacy to transient climate change. *J. Climate*, **23**, 2333–2344, https://doi.org/10.1175/2009JCLI3139.1.

——, S. M. Griffies, B. L. Samuels, J. L. Sarmiento, and T. L. Frölicher, 2013: Connecting changing ocean circulation with changing climate. *J. Climate*, **26**, 2268–2278, https://doi.org/10.1175/JCLI-D-12-00296.1.

Xie, P., and G. K. Vallis, 2012: The passive and active nature of ocean heat uptake in idealized climate change experiments. *Climate Dyn.*, **38**, 667–684, https://doi.org/10.1007/s00382-011-1063-8.

Xie, S.-P. 2020: Ocean warming pattern effect on global and regional climate change. *AGU Advances*, **1**, e2019AV000130, https://doi.org/10.1029/2019AV000130.

Xie, S.-P., C. Deser, G. A. Vecchi, J. Ma, H. Teng, and A. T. Wittenberg, 2010: Global warming pattern formation: Sea surface temperature and rainfall. *J. Climate*, **23**, 966–986, https://doi.org/10.1175/2009JCLI3329.1.

Yoshimori, M., and A. J. Broccoli, 2008: Equilibrium response of an atmosphere–mixed layer ocean model to different radiative forcing agents: Global and zonal mean response. *J. Climate*, **21**, 4399–4423, https://doi.org/10.1175/2008JCLI2172.1.

Zhou, C., M. D. Zelinka, and S. A. Klein, 2017: Analyzing the dependence of global cloud feedback on the spatial pattern of sea surface temperature change with a Green's function approach. *J. Adv. Model. Earth Syst.*, **9**, 2174–2189, https://doi.org/10.1002/2017MS001096.

Zhou, W., S. P. Xie, and D. Yang, 2019: Enhanced equatorial warming causes deep-tropical contraction and subtropical monsoon shift. *Nat. Climate Change*, **9**, 834–839, https://doi.org/10.1038/s41558-019-0603-9.